Temperature-Dependent Localized Excitations of Doped Carriers in Superconducting Diamond

K. Ishizaka,[1] R. Eguchi,[1] S. Tsuda,[2] A. Chainani,[3] T. Yokoya,[4] T. Kiss,[1] T. Shimojima,[1] T. Togashi,[3] S. Watanabe,[1] C.-T. Chen,[5] Y. Takano,[2] M. Nagao,[2] I. Sakaguchi,[2] T. Takenouchi,[6] H. Kawarada,[6] and S. Shin[1,3]

[1]*Institute for Solid State Physics, University of Tokyo, Kashiwa, Chiba 277-8581, Japan*
[2]*National Institute for Materials Science, Tsukuba, Ibaraki 305-0047, Japan*
[3]*The Institute of Physical and Chemical Research (RIKEN), Sayo-gun, Hyogo 679-5143, Japan*
[4]*The Graduate School of Natural Science and Technology, Okayama University, Okayama 700-8530, Japan*
[5]*Beijing Center for Crystal R&D, Chinese Academy of Science, Zhongguancun, Beijing 100080, China*
[6]*School of Science and Engineering, Waseda University, Shinjuku, Tokyo 169-8555, Japan*

(Received 28 August 2007; published 25 April 2008)

Laser-excited photoemission spectroscopy is used to show that the doped carriers in metallic or superconducting diamond couple strongly to the lattice via high-energy (~ 150 meV) optical phonons, with direct observations of localized Franck-Condon multiphonon sidebands appearing as Fermi-edge replicas. It exhibits a temperature-dependent spectral weight transfer from higher to lower energy sidebands and zero-phonon Fermi-edge states. The quantified coupling strength shows a systematic increase on lowering temperature, implicating its relation to the normal state transport and superconductivity.

DOI: 10.1103/PhysRevLett.100.166402 PACS numbers: 74.70.−b, 71.38.−k, 73.61.Cw, 79.60.−i

Diamond is an excellent electrical insulator with a wide band gap of 5.5 eV, but it is also a very good thermal conductor. Its thermal conductivity and superlative hardness is derived from sp^3 bonding, leading to high-energy optical phonons (HOPs) and a Debye temperature of 1860 K. Boron (B) doping results in high mobility p-type shallow acceptor states at 0.37 eV in the band gap. On increasing B concentration (n_B), the system undergoes an insulator-metal transition at $n_B^{\mathrm{MI}} \sim 2 \times 10^{20}$ cm^{-3} ($\sim 0.1\%$ substitution), followed by a striking emergence of superconductivity [1,2]. There is a growing consensus from experiment that superconductivity in B-doped diamond (BDD) is of the conventional BCS (Bardeen-Cooper-Schrieffer) type, with HOPs as the pairing glue [3–6]. However, the coupling of dilute carriers with such high-energy phonons of ~150 meV, theoretically discussed as the origin of superconductivity [7–11], is unique: it questions the validity of the adiabatic approximation [8,12] and awaits direct experimental proof. Also, strong randomness arising from site substitution of dopants manifests in high ($\sim$ mΩ cm) resistivity of the normal state, with a negative temperature (T) coefficient of resistance up to 300 K [1,3,14].

Photoelectron spectroscopy (PES) is a powerful probe of the electronic structure of a solid, in which an incident photon gets absorbed by the solid and results in removing an electron: an N-electron system goes to an $N-1$ electron system. In the sudden approximation, and for sufficiently weak interactions allowing a one-particle description of the N electrons, the photoelectron spectrum shows δ-function-like peaks for each initial state of the N-electron system. In contrast, for a strongly interacting system [e.g., electron-phonon (e-ph), e-e, etc.], several excited states can contribute to the $N-1$ final state and result in a multiple-peak spectrum for an initial state. A well-known example is the PES of gas molecules [15,16]. The PES of H_2 molecules [15] shows multiple peaks, consisting of a "0-0" peak at a kinetic energy (E_k) of E_0 and sidebands at $E_k = E_0 - n\omega_0$, where ω_0 is a characteristic vibrational energy of H_2 molecules (see Fig. 1 for schematics). The intensities of the multiple peaks are given

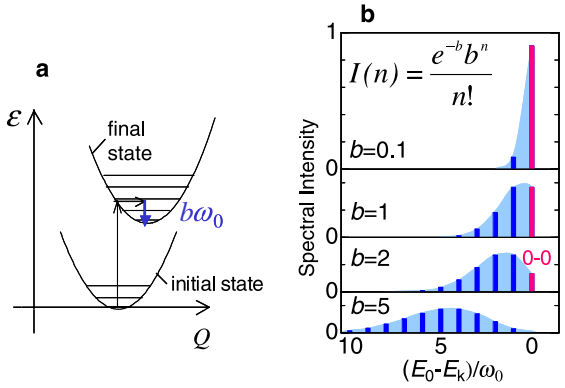

FIG. 1 (color online). (a) is a schematic of adiabatic potential curves with quantized phonon levels, for the initial and final (ionized) states. The PES spectral intensity from this model shows characteristic sidebands obeying the Franck-Condon factor, i.e., Poisson distribution [17], shown by blue (black) bars in (b). Here, b is the e-ph coupling parameter, corresponding to the number of phonons that can compensate the relaxation energy, $b\omega_0$. The "0-0" peak (zero-phonon line) at $E_k = E_0$ corresponds to a transition between the equilibrium states of the initial (e.g., H_2) and of the final (e.g., H_2^+) state system, where as the sidebands at $E_k = E_0 - n\omega_0$ reflect the transitions to vibrationally excited states. A light blue (gray) shaded area shows the envelope of the Poisson distribution.

by the Franck-Condon factor, i.e., a Poisson distribution. Such a characteristic spectral line shape can be reproduced with a model considering localized electrons coupling to a harmonic oscillator [17]. More recently, the broad spectral shapes of valence band PES in transition metal compounds exhibiting charge order, e.g., $(TaSe_4)_2I$, Fe_3O_4, and layered high-T_c cuprates [18–21], were explained in terms of the envelope of multiphonon sidebands arising from strong e-ph coupling [see Fig. 1(b)]. Phonon sidebands have been theoretically predicted in PES of polaronic materials [22,23]. A clear evidence of phonon sidebands in valence band PES, however, has not been reported to date.

PES measurements were performed using a system constructed with the VG-Scienta R4000 electron analyzer and an ultraviolet ($h\nu = 6.994$ eV) laser for the incident light [24]. The BDD samples used for measurements are characterized in Table I. BDD1 is a single crystal grown by high-pressure high-temperature synthesis, while other heavily doped samples are polycrystalline thin films grown by a microwave plasma CVD method as described elsewhere [14]. The pressure of the chamber during measurements was below 5×10^{-11} Torr. We annealed the samples at 400 °C in the vacuum of 1×10^{-7} Torr before measurements, following the surface cleaning procedure which removes the surface adsorbates while retaining the hydrogen termination [25,26], so as to obtain a surface free of contamination and reconstruction. The energy resolution was $\Delta E = 3.7$ meV. The Fermi level (E_F) of the sample was referred to that of a Au film evaporated on the sample substrate. For BDD1, which is still highly insulating, the measurement was performed at room temperature (RT) to avoid the effect of charging.

Figure 2 shows the n_B dependence of the PES at 4 K for samples BDD1–BDD4 (see Table I for details). The PES for the BDD1 sample shows a long tail-like spectrum without any evidence of a Fermi edge, indicative of a disordered p-type semiconductor. For BDD2 on the other hand, which is just on the verge of the insulator-metal transition, we already observe a small-step feature, indicative of a weak Fermi edge. The appearance and the evolution of the Fermi edge on B doping are clear in the magnified spectra plotted in Fig. 2. In the inset to Fig. 2, we plot the ratio of the intensity at the E_F to that at a binding energy (E_B) of 0.6 eV, so as to obtain a relative measure of the carrier number from the intensity at E_F. A rapid growth of the carrier number across the insulator (I)—metal (M)—superconductor (SC) transitions is evident, confirming a degenerate metal behavior for samples doped above the insulator-metal transition ($n_B > n_B^{\mathrm{MI}}$). For the metallic samples, we also recognize steplike features at around $E_B = 150$, 300, and 450 meV, in addition to the Fermi edge. Apparently, a periodicity in energy steps of $150 \times n$ meV ($n = 1$, 2, 3, and so on) is clear, and the steps are most prominent in the highest n_B sample, i.e., superconducting BDD4. Such periodic structures are possibly multiphonon sidebands emerging as replicas of the Fermi edge due to e-ph coupling. The optical phonon branches in pure diamond are well known, and correspond to the bond stretching vibration mode which is triply degenerate at Γ point with an energy of 164 meV [27]. It gives rise to a unique optically allowed phonon mode (A_g) in Raman scattering spectra. On increasing the B concentration above n_B^{MI}, the phonon peak in the Raman spectrum becomes rapidly broad and asymmetric as it softens, and exhibits a Fano-type resonance [28]. A recent inelastic x-ray scattering study reports phonon softening (~ 7 meV) in a superconducting diamond sample with $T_c = 4.2$ K, observed around Γ point in the optical phonon dispersion [29]. An infrared reflectivity study on a superconducting BDD also shows a clear kinklike structure at $\sim$150 meV [5]. This indicates that the periodic steps in PES are due to strong coupling of the optical phonon ($\omega_{\mathrm{ph}} \sim 150$ meV) to the doped carriers, resulting in the multiphonon sidebands. This coupling behavior has been invoked in virtual crystal approximation (VCA) [7,8] and supercell [9–11] numerical calculations which discuss a BCS-type superconductivity in BDD.

TABLE I. Characterization of the B-doped diamond samples.

Sample	n_B [cm^{-3}] (B/C%)	Electrical property	Synthesis
BDD1	3.5×10^{19} (0.02)	Insulating	HPHTS
BDD2	1.75×10^{20} (0.10)	Weakly insulating	CVD
BDD3	1.88×10^{21} (1.1)	SC, $T_c = 3.5$ K	CVD
BDD4	6.53×10^{21} (3.7)	SC, $T_c = 5$ K	CVD

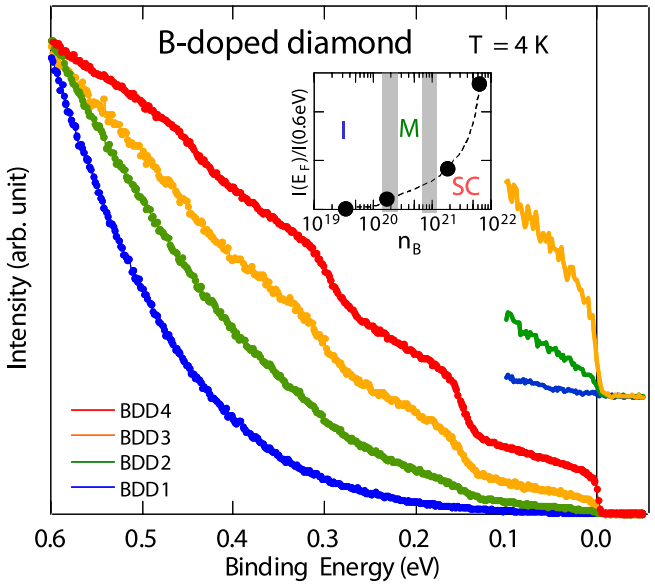

FIG. 2 (color online). The PES results showing the doping dependence of electronic structure for BDD1-4. Near-E_F region for BDD1-BDD3 is magnified in the upper part. The inset shows the intensity at E_F of PES normalized at 0.6 eV, as a function of n_B. I, M, and SC stand for insulator, metal, and superconducting phases as the ground state, respectively.

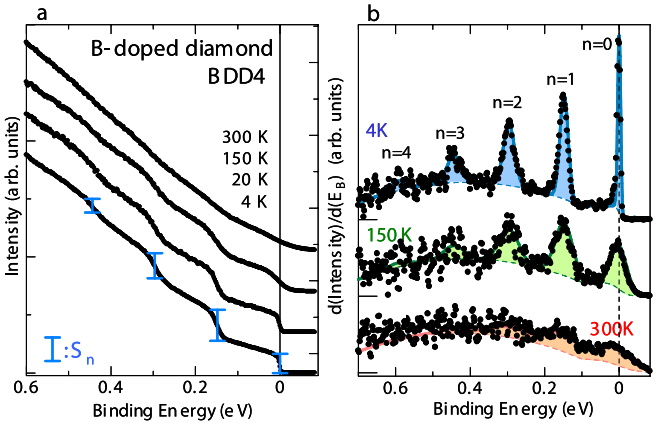

FIG. 3 (color online). The raw PES is shown in (a), while (b) shows the E_B derivative of PES. The solid (broken) curves in (b) indicate the fitting function (background) for respective T. The bars in (a) indicate the sideband intensities S_n, obtained by the analysis on the E_B-derivative curves in (b).

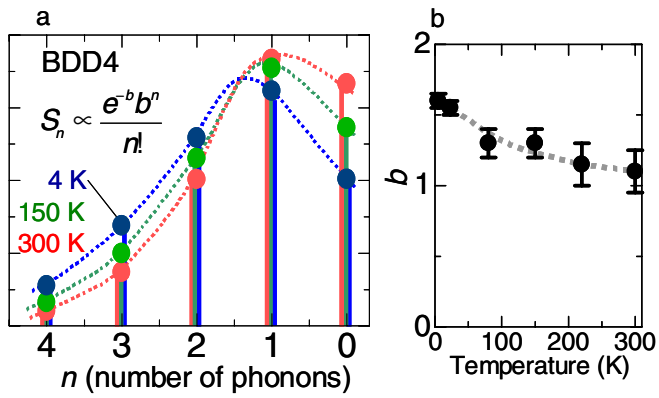

FIG. 4 (color online). (a) T dependence of sideband intensities S_n obtained by the analysis on BDD4. The broken curves are guides for eyes to show the envelope of the Poisson distribution. (b) shows the T dependence of the e-ph coupling factor b.

In the following, we analyze these multiphonon sidebands in close detail for the most heavily doped BDD4. The T-dependent PES are shown in Fig. 3(a). Comparing spectra at 4 and 20 K, the sidebands at $150 \times n$ meV are scarcely modified across the superconducting transition temperature $T_c \sim 5$ K. At higher T, the sidebands become blurred as the Fermi edge gets smeared due to the Fermi-Dirac distribution. To see this more clearly, we show in Fig. 3(b), the first E_B derivative of the photoemission spectra [30]. The steplike features in the raw data [Fig. 3(a)] now appear as well-defined peak structures in the derivative spectra of Fig. 3(b). At 300 K, the periodic peak structures are still discernible up to $n = 2$. To account for the multiphonon sidebands, we applied the Franck-Condon analysis. We first fitted the spectrum at 4 K with a proper background function $I_{\mathrm{BG}}(E_B)$ shown by the broken curve and a set of normalized Gaussian curves $g(E_B - n\omega_0, W_n)$ with peaks at $E_B = n\omega_0$ and the half-width-half-maximum (HWHM) W_n as $I(E_B) = I_{\mathrm{BG}}(E_B) + \sum_n S_n g(E_B - n\omega_0, W_n)$. For W_n, we assumed the relation $W_n = \sqrt{W_0^2 + nW_{\mathrm{ph}}^2}$, representing the n-times convolution of the phonon Gaussian spectrum to the Fermi-edge-derived Gaussian component with HWHM of W_0. We further fix the nth peak integrated intensity S_n to follow the Poisson distribution, $S_n \propto \frac{e^{-b}b^n}{n!}$. The result of fitting is plotted in Fig. 3(b), with the parameters $b = 1.6$, $\omega_0 = 148$ meV, $W_0 = 4.8$ meV, and $W_{\mathrm{ph}} = 12$ meV, showing an excellent fit to the data. The "0-0" peak or the zero-phonon line now corresponds to the Fermi-edge derived peak at E_F. Here, the factor b is the effective e-ph coupling parameter. The obtained integrated intensities S_n are indicated as a function of n in Fig. 4(a). Since S_n corresponds to the heights of the steplike structures (Fermi-edge replicas) in the raw PES, we also plotted them at $148n$ meV along with the 4 K raw PES in Fig. 3(a) for a consistency check. Since $b = 1.6 > 1$, the $n = 1$ sideband integrated intensity is greater than that of the zero-phonon line. It indicates a suppression of the zero-phonon line and a phonon dressing of carriers.

The applicability of Franck-Condon analyses for the multiphonon sidebands in BDD clearly shows that they are created in an optical excitation process and indicates that the adiabatic approximation is valid for the coupling of carriers with HOPs [31]. It is surprising that a simple localized e-ph model is applicable for carriers in a metal undergoing a superconducting transition. One possibility to phenomenologically deal with such "localized carriers" is the small polaron picture, previously discussed for the broad PES line shape in transition metal compounds [18–21]. As stated, theoretical calculations for polaronic systems have predicted periodic oscillations in the PES spectrum near-E_F [22,23], especially when the coupling phonon dispersion shows high-energy and flat characteristics [22]. This seems the likely picture for metallic diamond, and may explain this first observation of phonon-derived oscillations in near-E_F PES. We believe this unique nature of the carrier-phonon coupling leads to the superconductivity in doped diamond.

We have further carried out a similar fitting analysis to study the T dependence of multiphonon sidebands. Since the phonon energy $\omega_0 = 148$ meV is much greater than the energy scale of RT (300 K $\sim$ 25 meV), we assumed that the thermal effect on the phonon energy can be ignored, thereby fixing ω_0 and W_{ph} for all T. We varied b as a function of T, and also adjusted W_0 and the edge component in the background to follow the Fermi-Dirac statistics. The results of the fitting are shown in Fig. 3(b) and give $b = 1.3$ and 1.1 for 150 K and 300 K. Corresponding S_n are shown in Fig. 4(a) as a function of n, and the T dependence of b is plotted in Fig. 4(b). On increasing T, b tends to get smaller indicating the transfer of spectral weight from higher to lower E_B sidebands, i.e., recovery of the zero-phonon line. In other words, the e-ph

coupling constant b systematically increases on reducing T. Since HOP characteristics and population are not expected to change significantly up to 300 K, this T dependence must be electronic in origin. Indeed, the T dependence of b resembles that of the normal state resistivity [1,3,14], with a negative T coefficient observed up to 300 K. At $T < 20$ K in the normal phase, the resistivity follows a $T^{-1/2}$ behavior reflecting a disordered Fermi liquid with long-range Coulomb interactions [6]. While studies at high T above RT are necessary for obtaining a comprehensive microscopic description of the wide-T transport properties in superconducting diamond, the localized Franck-Condon excitations would reflect the carrier property via the changes observed for the zero-phonon Fermi-edge states. The increase in b on reducing T must be thus related to the resistivity behavior indicative of a progressively stronger renormalization of states at E_F, and consequently leads to superconductivity in BDD. The results thus show the unusual relation of localized excitations with doped charge carriers which undergo a superconducting transition. This is quite unexpected in a conventional superconductor, and suggests the need of further theoretical studies that go beyond conventional mechanisms.

In conclusion, we have studied the boron-doped diamond by laser-excited photoemission spectroscopy. We found the evolution of Fermi edge on increasing the doping level above insulator-metal transition. In metallic samples, the clear multiphonon sidebands were observed for the first time in PES of solid. The T dependence of the sidebands shows the increase of electron-phonon coupling on lowering T, which suggests its possible relation to the carrier transport and thus superconductivity.

We thank Y. Kayanuma, H. Fukuyama, O. Gunnarsson, K. Nasu, E. Bustarret, and Y. Takada for fruitful discussions.

[1] E. A. Ekimov *et al.*, Nature (London) **428**, 542 (2004).
[2] E. Bustarret *et al.*, Phys. Rev. Lett. **93**, 237005 (2004).
[3] V. A. Sidorov, E. A. Ekimov, S. M. Stishov, E. D. Bauer, and J. D. Thompson, Phys. Rev. B **71**, 060502(R) (2005).
[4] B. Sacepe *et al.*, Phys. Rev. Lett. **96**, 097006 (2006).
[5] M. Ortolani *et al.*, Phys. Rev. Lett. **97**, 097002 (2006).
[6] K. Ishizaka *et al.*, Phys. Rev. Lett. **98**, 047003 (2007).
[7] L. Boeri, J. Kortus, and O. K. Andersen, Phys. Rev. Lett. **93**, 237002 (2004).
[8] K. W. Lee and W. E. Pickett, Phys. Rev. Lett. **93**, 237003 (2004).
[9] X. Blase, Ch. Adessi, and D. Connetable, Phys. Rev. Lett. **93**, 237004 (2004).
[10] H. J. Xiang, Z. Li, J. Yang, J. G. Hou, and Q. Zhu, Phys. Rev. B **70**, 212504 (2004).
[11] F. Giustino, R. Yates Jonathan, I. Souza, M. L. Cohen, and G. Louie, Phys. Rev. Lett. **98**, 047005 (2007).
[12] When the ratio of the characteristic carrier kinetic energy to the phonon energy is small, $\omega_{\mathrm{ph}}/E_F \ll 1$, the adiabatic assumption (Eliashberg-Migdal approximation) should be valid. Since ω_{ph}/E_F is expected to be considerably large in this system (order of $0.1 \sim 1$ with $\omega_{\mathrm{ph}} = 0.15$ eV and $E_F \sim 0.4$ eV [13]) compared to conventional metals ($< 10^{-3}$), nonadiabatic effects can become important.
[13] T. Yokoya *et al.*, Nature (London) **438**, 647 (2005).
[14] Y. Takano *et al.*, Appl. Phys. Lett. **85**, 2851 (2004); Y. Takano *et al.*, Diam. Relat. Mater. **14**, 1936 (2005).
[15] L. Åbsrink, Chem. Phys. Lett. **7**, 549 (1970).
[16] F.-J. Himpsel, N. Schwentner, and E. E. Koch, Phys. Status Solidi B **71**, 615 (1975).
[17] G. D. Mahan, *Many-Particle Physics* (Plenum, New York, 1981).
[18] L. Perfetti *et al.*, Phys. Rev. Lett. **87**, 216404 (2001).
[19] K. M. Shen *et al.*, Phys. Rev. Lett. **93**, 267002 (2004).
[20] D. Schrupp *et al.*, Europhys. Lett. **70**, 789 (2005).
[21] O. Rosch *et al.*, Phys. Rev. Lett. **95**, 227002 (2005).
[22] A. S. Alexandrov and J. Ranninger, Phys. Rev. B **45**, 13109 (1992).
[23] V. Perebeinos and P. B. Allen, Phys. Rev. Lett. **85**, 5178 (2000).
[24] T. Kiss *et al.*, Phys. Rev. Lett. **94**, 057001 (2005).
[25] F. Maier, M. Riedel, B. Mantel, J. Ristein, and L. Ley, Phys. Rev. Lett. **85**, 3472 (2000); D. Takeuchi, M. Riedel, J. Ristein, and L. Ley, Phys. Rev. B **68**, 041304(R) (2003); M. Riedel, J. Ristein, and L. Ley, *ibid.* **69**, 125338 (2004).
[26] J. I. B. Wilson *et al.*, J. Electron Spectrosc. Relat. Phenom. **121**, 183 (2001).
[27] J. L. Warren, J. L. Yarnell, G. Dolling, and R. A. Cowley, Phys. Rev. **158**, 805 (1967).
[28] E. Bustarret, E. Gheeraert, and K. Watanabe, Phys. Status Solidi A **199**, 9 (2003).
[29] M. Hoesch *et al.*, Phys. Rev. B **75**, 140508(R) (2007).
[30] To decrease the noise level in the E_B-derivative curves, the PES have been smoothed in advance. Without the smoothing, the sidebands for $n > 3$ are hardly recognizable due to the enhanced noise. The parameters we obtained from the nonsmoothed PES are $b = 1.6$, $W_0 = 3.1$ meV, $W_{\mathrm{ph}} = 12$ meV, and $\omega_0 = 148$ meV. Note that solely W_0 is altered, which merely indicates the width of the Fermi-edge component.
[31] If the multiphonon sidebands were due to inelastic scattering of the excited (hot) electrons traveling on their way out through the solid [32], the intensity of the sidebands should have followed a power law $S_n = Aa^n$ with $a = \lambda_{\mathrm{tot}}/\lambda_{\mathrm{ph}} < 1$. Here, λ_{tot} and λ_{ph} are the total escape depth and the attenuation length due to phonon creation, respectively, of the hot electrons. From the observed Poisson distribution behavior, we can rule out this possibility.
[32] R. Arafune, K. Hayashi, S. Ueda, Y. Uehara, and S. Ushioda, Phys. Rev. Lett. **95**, 207601 (2005).